THE JOURNAL OF NAVIGATION (2017), **70**, 465–482.
doi:10.1017/S0373463316000771

Performance Evaluation of Single-frequency Precise Point Positioning with GPS, GLONASS, BeiDou and Galileo

Lin Pan[1,2], Xiaohong Zhang[1,2], Jingnan Liu[1], Xingxing Li[1,3] and Xin Li[1]

[1](*School of Geodesy and Geomatics, Wuhan University, Wuhan, China*)
[2](*Collaborative Innovation Center for Geospatial Technology, 129 Luoyu Road, Wuhan, China*)
[3](*German Research Centre for Geosciences* (*GFZ*)*, Telegrafenberg, Potsdam, Germany*)
(E-mail: xhzhang@sgg.whu.edu.cn)

In view that most Global Navigation Satellite System (GNSS) users are still using single-frequency receivers due to the low costs, single-frequency Precise Point Positioning (PPP) has been attracting increasing attention in the GNSS community. For a long period, single-frequency PPP technology has mainly relied on the Global Positioning System (GPS). With the recent revitalisation of the Russian GLONASS constellation and two newly emerging constellations, BeiDou and Galileo, it is now feasible to investigate the performance of Four-Constellation integrated Single-Frequency PPP (FCSF-PPP) with GPS, GLONASS, BeiDou and Galileo measurements. In this study, a FCSF-PPP model is presented to simultaneously process observations from all four GNSS constellations. Datasets collected at 47 globally distributed four-system Multi-GNSS Experiment (MGEX) stations on seven consecutive days and a kinematic experimental dataset are employed to fully assess the performance of FCSF-PPP. The FCSF-PPP solutions are compared to GPS-only and combined GPS/GLONASS single-frequency PPP solutions. The results indicate that the positioning performance is significantly improved by integrating multi-constellation signals.

KEYWORDS

1. Precise point positioning. 2. Single-frequency. 3. Four-constellation.

Submitted: 23 December 2015. Accepted: 12 October 2016. First published online 1 February 2017.

1. INTRODUCTION. The concept of Precise Point Positioning (PPP) was first proposed in the mid-1990s (Héroux and Kouba, 1995; Zumberge et al., 1997). The PPP technique is usually carried out with the use of dual-frequency code and carrier phase observations as well as the correction data from the precise satellite orbit and clock products (Kouba and Héroux, 2001). Over the past two decades, significant progress has been

achieved in dual-frequency PPP, which is currently able to provide millimetre-level accuracy in static mode and centimetre-level accuracy in kinematic mode (Li et al., 2011; 2013a). However, single-frequency Global Navigation Satellite System (GNSS) receivers are still widely used in most positioning and navigation applications due to the low costs (Øvstedal, 2002; Montenbruck, 2003). Therefore the development of a single-frequency PPP technique has aroused great interest in the GNSS community (Cai et al., 2013; Li et al., 2013b; Sterle et al., 2015).

In single-frequency PPP, proper handling of the ionospheric delay is a key issue. There are presently two main ways to solve this issue. One way is to apply ionospheric models, such as the Global Ionosphere Maps (GIM) ionospheric model and the Klobuchar model, to mitigate or eliminate the ionospheric effect (Øvstedal, 2002; Le and Tiberius, 2007; Li et al., 2013b). Another way is to use the code and carrier phase observations on a single frequency to form an ionosphere-free observable, which is known as the GRoup And PHase Ionospheric Correction (GRAPHIC) (Yunck, 1996; Montenbruck, 2003). Numerical results show that single-frequency PPP based on GRAPHIC can achieve centimetre-level accuracy in static mode and decimetre-level accuracy in kinematic mode, which is several times better than that of ionospheric mitigation models (Sterle et al., 2015). In this study, the GRAPHIC ionosphere-free linear combination is adopted to remove the ionospheric effect.

According to the above discussions, most of the research work about single-frequency PPP has focused on the correction of ionospheric delay and was carried out relying on the GPS system. Efforts were also made to improve the single-frequency PPP performance by combining GPS with GLONASS (Cai et al., 2013). The results demonstrated that both the positioning accuracy and convergence time were improved by approximately 30%. Moreover, the improvement in precision and convergence speed for dual-frequency PPP has been widely confirmed when observations from other GNSS systems are available in addition to GPS (Li et al., 2015a; 2015b; Cai et al., 2015; Pan et al., 2014). The joint use of multi-constellation signals has become a trend in GNSS development (Li et al., 2015a). Multi-constellation integrated single-frequency PPP has the potential to significantly improve positioning accuracy and reduce the position convergence time due to the increased number of visible satellites and the improved satellite sky distribution, especially when positioning is performed in areas with GNSS signal blockages.

GLONASS, BeiDou and Galileo systems have boomed in recent years. A full GLONASS constellation consisting of 24 operational satellites has been completely revitalised since 2012. BeiDou was declared to provide navigation and position services over the Asia-Pacific region with a constellation of 14 operational satellites on 27 December 2012. Four new generation BeiDou satellites were successfully launched on 30 March, 25 July and 30 September 2015, respectively, which marks the start of the BeiDou system expansion from regional to global scale. Currently the four new BeiDou satellites are still being commissioned. The Galileo constellation has had four In-Orbit Validation (IOV) satellites and four Full Operational Capability (FOC) satellites since 27 March 2015. GNSS users are able to simultaneously use four-constellation signals under the current GNSS constellations, which provides an opportunity to investigate the performance of Four-Constellation integrated Single-Frequency PPP (FCSF-PPP) with GPS, GLONASS, BeiDou and Galileo measurements. In this study, a FCSF-PPP model based on the GRAPHIC ionosphere-free linear combination is presented and its performance is investigated using the datasets collected at 47 globally distributed four-system Multi-GNSS

Experiment (MGEX) stations on seven consecutive days and a kinematic experimental dataset.

2. POSITIONING MODEL WITH FOUR CONSTELLATIONS. The pseudorange and carrier phase observations on L1/G1/B1/E1 frequencies are used, and they can be expressed as:

$$P_r^s = \rho_r^s + c(dt_r - dt^s) + d_{orb}^s + I_r^s + d_{r,trop}^s + c(b_r - b^s) + \varepsilon_{r,P}^s \quad (1)$$

$$L_r^s = \rho_r^s + c(dt_r - dt^s) + d_{orb}^s - I_r^s + d_{r,trop}^s + \lambda N_r^s + \lambda(d_r - d^s) + \varepsilon_{r,L}^s \quad (2)$$

where the indices s and r refer to the satellite and receiver, respectively. P is the measured pseudorange in metres, L is the measured carrier phase in metres, ρ is the geometric range between the phase centres of the satellite and receiver antennas in metres, c is the speed of light in a vacuum in metres per second, dt_r is the receiver clock offset in seconds, dt^s is the satellite clock offset in seconds, d_{orb} is the satellite orbit error in metres, I is the ionospheric delay in metres, d_{trop} is the tropospheric delay in metres, λ is the wavelength in metres, N is the phase ambiguity term in cycles, b_r and b^s are the code biases of the receiver and the satellite in seconds, d_r and d^s are the receiver- and satellite-dependent Uncalibrated Phase Delays (UPDs) in cycles, and ε is the observation noises including multipath in metres. The tropospheric delays are usually split into a hydrostatic (dry) and a non-hydrostatic (wet) part (Davis et al., 1985). The Saastamoinen (1972) tropospheric model is used to correct the dry part from the measurements whereas the wet part is estimated from the measurements. The Global Mapping Functions (GMF) (Boehm et al., 2006) are used to project the slant delays to the zenith delay.

Based on the GRAPHIC linear combination, the ionosphere-free combined observable Φ can be obtained by combining Equations (1) and (2). Φ can be described below:

$$\begin{aligned}\Phi_r^s = 0{\cdot}5(P_r^s + L_r^s) = {} & \rho_r^s + c(dt_r - dt^s) + d_{orb}^s + m_r^s \cdot Z_r + 0{\cdot}5\lambda N_r^s \\ & + 0{\cdot}5\lambda(d_r - d^s) + 0{\cdot}5c(b_r - b^s) + \varepsilon_{r,\Phi}^s \end{aligned} \quad (3)$$

where m is the wet mapping function, and Z_r is the tropospheric Zenith Wet Delay (ZWD) at the station r in metres.

In order to investigate the emerging new navigation systems such as BeiDou and Galileo, MGEX has been established by the International GNSS Service (IGS) to serve as a platform (Rizos et al., 2013). Four-constellation mixed precise satellite orbit file "gbmwwwwd.sp3" and clock file "gbmwwwwd.clk" are provided daily by GFZ, which is one of the MGEX analysis centres, are adopted for FCSF-PPP processing (Li et al., 2015b). The ionosphere-free linear combination of pseudorange $P1$ and $P2$ is usually used for the generation of precise satellite clock products, but the code biases are ignored during the estimation process. As such, the satellite clock correction dt_I^s provided in the precise satellite clock products contains a specific linear combination of satellite code biases in $P1$ and $P2$ (Guo et al., 2015), which can be shown as follows:

$$dt_I^s = dt^s + cb_{IF}^s \quad (4)$$

$$b_{IF}^s = \frac{f_1^2 \cdot b_1^s - f_2^2 \cdot b_2^s}{f_1^2 - f_2^2} \quad (5)$$

https://doi.org/10.1017/S0373463316000771 Published online by Cambridge University Press

where f_1 and f_2 are two carrier-phase frequencies in Hertz. b_1^s and b_2^s are the code biases on the satellite end in $P1$ and $P2$ in seconds, respectively.

After applying the precise satellite orbit and clock corrections, the ionosphere-free observable Φ can be rewritten as:

$$\Phi_r^s = \rho_r^s + cdt_r + m_r^s \cdot Z_r + 0{\cdot}5\lambda N_r^s + B_r^s + \varepsilon_{r,\Phi}^s \tag{6}$$

$$B_r^s = 0{\cdot}5\lambda(d_r - d^s) + 0{\cdot}5c(b_r + 2b_{IF}^s - b_1^s) \tag{7}$$

where B is a linear combination of code biases and phase delays on the receiver and satellite ends, and B can be decomposed into an average term B_α and a satellite-dependent bias term δB as given below:

$$B_r^s = B_{r,\alpha}^s + \delta B_r^s \tag{8}$$

The average term B_α and the satellite-dependent bias term δB will be absorbed into the receiver clock and phase ambiguity items, respectively, in the parameter estimation process. Equation (6) can then be rewritten as:

$$\Phi_r^s = \rho_r^s + c\widetilde{dt}_r + m_r^s \cdot Z_r + 0{\cdot}5\lambda\widetilde{N}_r^s + \varepsilon_{r,\Phi}^s \tag{9}$$

$$\widetilde{dt}_r = dt_r + B_{r,\alpha}^s/c \tag{10}$$

$$\widetilde{N}_r^s = N_r^s + 2\delta B_r^s/\lambda \tag{11}$$

To ensure accuracy and reliability, the Differential Code Biases (DCB) products can also be used for code bias corrections. Currently both the receiver-specific code biases for MGEX stations and the satellite-specific code biases for GPS, GLONASS, BeiDou and Galileo are provided by MGEX in the annual files "MGEXyyyy.bsx" and "MGEXyyyy_all.bsx" (Guo et al., 2015).

The FCSF-PPP observation model can be depicted as:

$$\Phi_r^G = \rho_r^G + c\widetilde{dt}_{rG} + m_r^G \cdot Z_r + 0{\cdot}5\lambda_G\widetilde{N}_r^G + \varepsilon_{r,\Phi}^G \tag{12}$$

$$\Phi_r^R = \rho_r^R + c\widetilde{dt}_{rR} + m_r^R \cdot Z_r + 0{\cdot}5\lambda_R\widetilde{N}_r^R + \varepsilon_{r,\Phi}^R \tag{13}$$

$$\Phi_r^C = \rho_r^C + c\widetilde{dt}_{rC} + m_r^C \cdot Z_r + 0{\cdot}5\lambda_C\widetilde{N}_r^C + \varepsilon_{r,\Phi}^C + b_{sys}^C \tag{14}$$

$$\Phi_r^E = \rho_r^E + c\widetilde{dt}_{rE} + m_r^E \cdot Z_r + 0{\cdot}5\lambda_E\widetilde{N}_r^E + \varepsilon_{r,\Phi}^E \tag{15}$$

where the superscripts G, R, C and E refer to GPS, GLONASS, BeiDou and Galileo satellites, respectively. The four receiver clock offset parameters in Equations (12)–(15) are different because the code biases and phase delays partially absorbed by them are different for different satellite systems (Li et al., 2015a). In the precise products provided by GFZ, the time scales of the four GNSS systems are unified to the GPS time. The different receiver clock offsets should not be attributed to the system time offsets between GNSS systems. Hence, the unknown parameters include three receiver coordinates, four receiver clock offsets, one tropospheric ZWD, and real-valued ambiguity parameters equal to the number of the observed GPS, GLONASS, BeiDou and Galileo satellites. In Equation (14), b_{sys} is the unique systematic bias in BeiDou code observations. The code observations from BeiDou Geostationary Orbit (GEO) satellites are down-weighted to weaken the effects of the systematic biases in this study. As to BeiDou Inclined Geosynchronous Orbit (IGSO)

https://doi.org/10.1017/S0373463316000771 Published online by Cambridge University Press

and Medium Earth Orbit (MEO) satellites, the elevation-dependent correction model for code systematic biases is adopted (Wanninger and Beer, 2015).

The file "igs08_wwww.atx" generated and released by IGS is used to correct the GPS and GLONASS satellite Phase Centre Offsets (PCOs) and Variations (PCVs). The antenna offsets recommended by MGEX are used to correct the PCOs of BeiDou and Galileo satellites, while the BeiDou and Galileo PCV corrections are still unavailable (Rizos et al., 2013). As other error mitigations have been well described in work such as Kouba and Héroux (2001), they will not be covered again.

Since a Kalman filter is applied for FCSF-PPP, appropriate stochastic models for the measurements and dynamic models for the parameters need to be provided. As can be seen from Equation (3), the GRAPHIC ionosphere-free combined observations are a linear combination of the original code and phase measurements. Assuming that there is no correlation between the two types of measurements, the initial variances of the ionosphere-free observations can be obtained by applying the law of random error propagation as follows:

$$\sigma_{\Phi}^2 = 0{\cdot}25\sigma_P^2 + 0{\cdot}25\sigma_L^2 \approx 0{\cdot}25\sigma_P^2 \tag{16}$$

where σ_P^2 and σ_L^2 are the variances of code and phase observations, respectively. The variance of phase observations is far smaller than that of code observations, and thus can be neglected. The actual variances are defined as a function of the initial variances and the satellite elevation angles (Gerdan, 1995).

As to the dynamic models for the unknown parameters, the ambiguity parameters and static receiver coordinates are modelled as constants, while the receiver clock offsets and kinematic receiver coordinates may be modelled as a Random Walk (RW) or a first-order Gauss–Markov process. The ZWD can be modelled as a RW process (Cai et al., 2015).

In the specific implementation of FCSF-PPP dynamic and stochastic models, the spectral density values for the receiver clock offsets and ZWD are empirically set to 10^5 and 10^{-9} m^2/s, respectively. In kinematic mode, a value of 10^2 m^2/s is set as the spectral density value for receiver coordinates. The precision of the GPS code observations is set to 0·3 m (Pan et al., 2014). The precision of the GLONASS code observations is set to 0·6 m partly because of its higher code noise level. The higher code measurement noises of GLONASS are due to its lower code chipping rate equal to half that of GPS code observations (Hauschild et al., 2012; Montenbruck, 2003). In addition, the satellite-specific receiver code biases may also contribute to the down-weighting of GLONASS code observations. Since the accuracy of BeiDou and Galileo satellite orbits and clocks are relatively lower than GPS (Zhao et al., 2013; Steigenberger et al., 2015), their measurements are down-weighted. The precision of code observations is set to 0·6 m for Galileo, BeiDou IGSO and MEO satellites, while the code observation precision of BeiDou GEO satellites is set to 0·9 m.

3. RESULTS AND ANALYSIS.

3.1. *Data description.* Datasets collected at 47 globally distributed four-system MGEX stations on 1–7 April 2015 are used to assess the performance of FCSF-PPP. The geographical distribution of the selected stations is shown in Figure 1. All selected stations were equipped with multi-GNSS receivers which can produce GPS, GLONASS, BeiDou and Galileo observations. All observations were post-processed and recorded at a sampling

https://doi.org/10.1017/S0373463316000771 Published online by Cambridge University Press

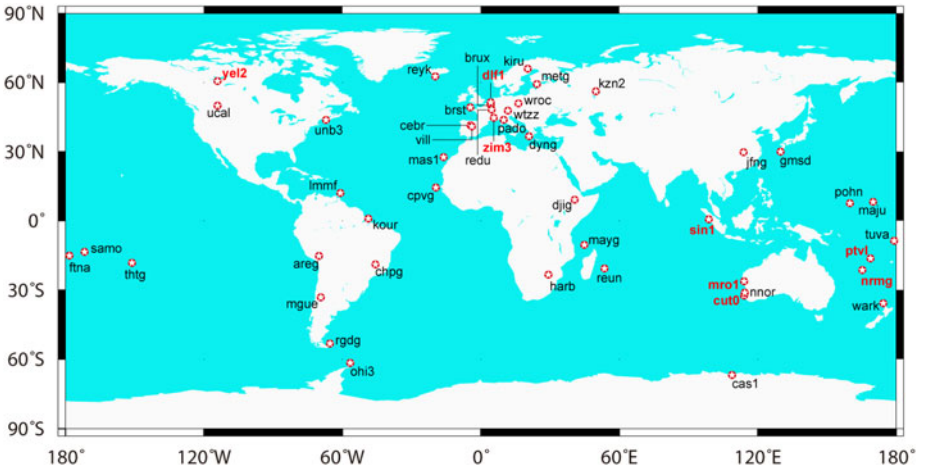

Figure 1. Geographical distribution of 47 four-system MGEX stations.

interval of 30 s. The satellite elevation mask angle was set to 10°. Since the precise coordinates of eight selected MGEX stations, which are marked in red in Figure 1, are not available in file "igs15Pwwwwd.snx" provided by IGS, their coordinate values are computed through an Online Positioning User Service (OPUS), which is capable of providing centimetre-level or even millimetre-level positioning accuracy (Ghoddousi-Fard and Dare, 2006) and available at: http://www.ngs.noaa.gov/OPUS. As the repeatability of the OPUS processing results is at a millimetre-level from day to day, the average differential positioning results over the seven days are used to assess the single-frequency PPP solutions at the eight stations. In order to assess the OPUS processing results, the station coordinates that are available in SINEX solutions are re-computed using the OPUS. The difference between the SINEX solutions and the average OPUS solutions over seven days is 1–3 mm.

3.2. *FCSF-PPP result analysis.* In order to investigate the performance improvement attributing to multi-constellation integration, the dataset from station JFNG on 7 April 2015 is processed in different constellation combinations, i.e. GPS-only, GPS/GLONASS and GPS/GLONASS/BeiDou/Galileo. The station JFNG is located in Wuhan, China and covered by the BeiDou service of the Asia-Pacific area. Figure 2 shows the epoch-wise positioning errors for the three different combination cases. Compared with the GPS-only case, GPS/GLONASS single-frequency PPP achieves better convergence performance, especially in the vertical coordinate component. The convergence time is further reduced after adding BeiDou and Galileo observations. As to positioning accuracy, the Root Mean Square (RMS) values of position errors over the last 15 minutes are 0·3, 2·0 and 1·5 cm for four-constellation case in the east, north and up directions, respectively. The above accuracy is better than that of GPS-only and GPS/GLONASS cases, which are 0·4, 2·8 and 3·1 cm, and 0·4, 2·2 and 1·7 cm in the three directions, respectively. Figure 3 presents the number of visible satellites and Position Dilution of Precision (PDOP) for each processing case. It is clear that multi-constellation integration significantly increases the number of visible satellites and simultaneously decreases the PDOP values. The average satellite numbers and PDOP values for the above three processing cases are 8·1, 14·6 and 25·7, and 2·0, 1·5 and 1·2, respectively. In conjunction with the position solutions, it is concluded

https://doi.org/10.1017/S0373463316000771 Published online by Cambridge University Press

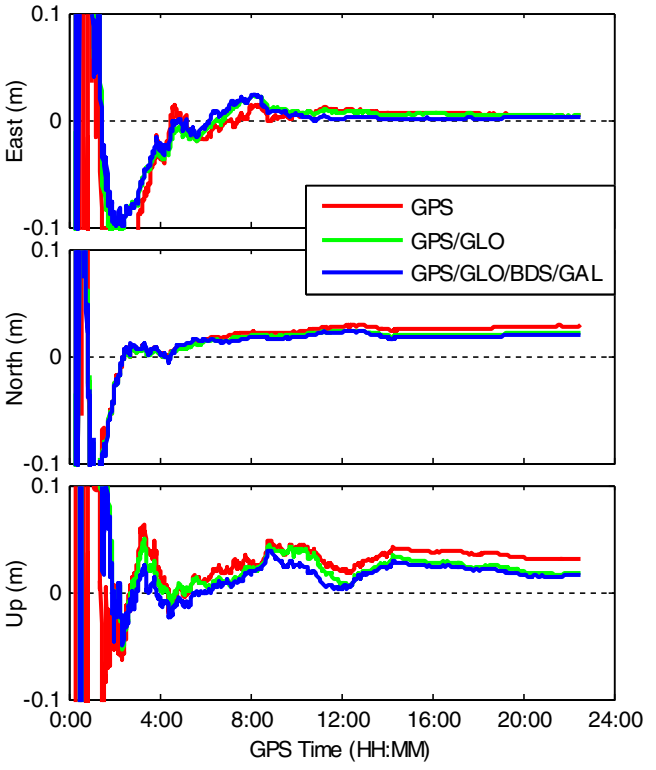

Figure 2. Single-frequency PPP positioning errors for three different constellation combinations at JFNG on 7 April 2015. The abbreviations GLO, BDS and GAL represent GLONASS, BeiDou and Galileo, respectively.

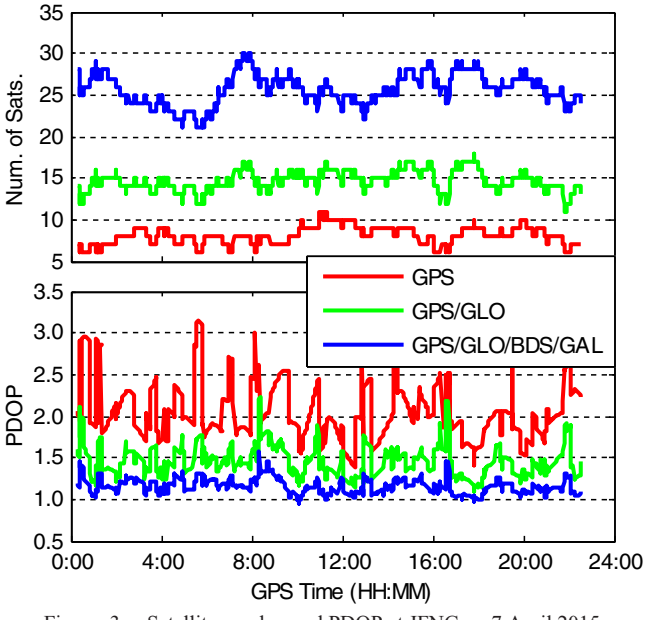

Figure 3. Satellite number and PDOP at JFNG on 7 April 2015.

https://doi.org/10.1017/S0373463316000771 Published online by Cambridge University Press

that the performance of multi-constellation integrated single-frequency PPP benefits from the increased number of satellites and improved satellite sky distribution.

Since observation residuals contain measurement noises and other unmodelled errors, they can also be used as an important index to evaluate the FCSF-PPP model. Figure 4 shows the observation residuals in the four-constellation integrated processing case. Different colours represent different satellites. As can be seen, most GPS, GLONASS and BeiDou observation residuals vary within a similar range of $-0{\cdot}5\,\mathrm{m} \sim 0{\cdot}5\,\mathrm{m}$, whereas the Galileo observation residuals vary in a significantly smaller range. There are almost no observation residuals for Galileo when only one Galileo satellite is available. This is because two more unknown parameters, namely Galileo receiver clock offset and phase ambiguity, need to be estimated after adding one Galileo measurement. The RMS statistics are also displayed in each panel. The statistical results clearly demonstrate that GLONASS has the largest observation residuals with 0·161 m, while Galileo has the smallest observation residuals with 0·084 m. GPS and BeiDou observation residuals are comparable with values of 0·130 m and 0·136 m, respectively. Since observation residuals show a comprehensive effect of remaining satellite orbit and clock error, ranging error, ionospheric delay error and other unmodelled errors, they are different for different constellations. The smallest observation residuals from Galileo are partly due to the lower measurement redundancy and the higher satellite elevation angles. Overall, the RMS residuals are smaller than 0·17 m for

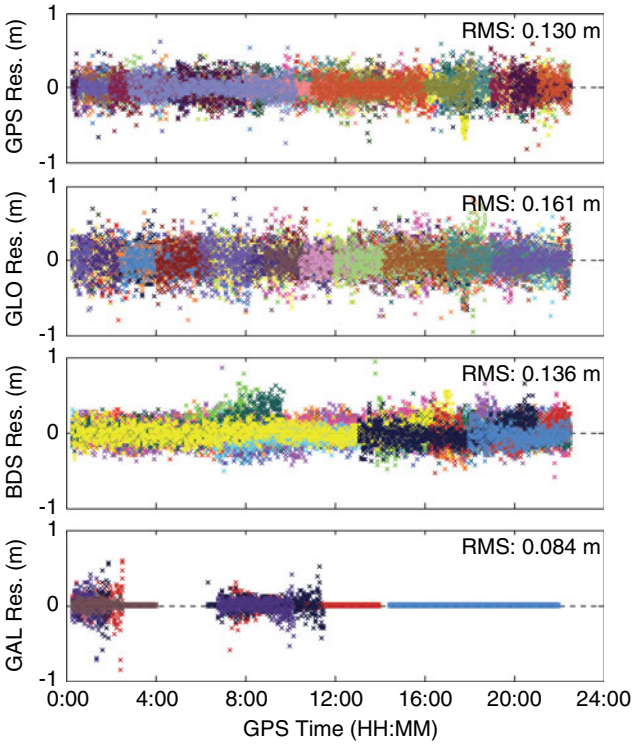

Figure 4. Observation residuals for FCSF-PPP at JFNG on 7 April 2015.

https://doi.org/10.1017/S0373463316000771 Published online by Cambridge University Press

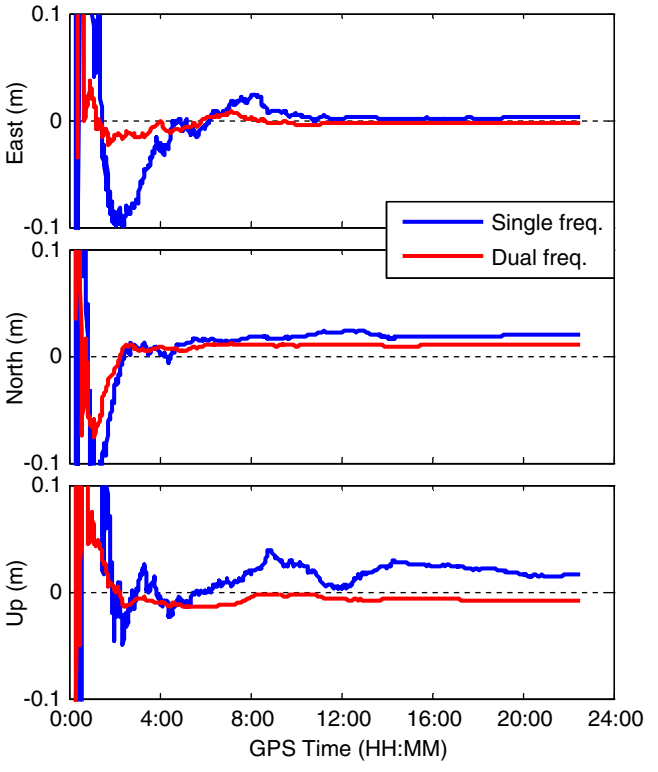

Figure 5. Single-frequency vs. dual-frequency PPP position errors using combined GPS, GLONASS, BeiDou and Galileo observations at JFNG on 7 April 2015.

all four GNSS systems and no systematic errors can be found in the residuals, suggesting that various errors and biases in GRAPHIC ionosphere-free observations from different constellations have been properly handled in the FCSF-PPP model.

To compare the performance of single- and dual-frequency PPP, Figure 5 shows a comparison between FCSF-PPP and Four-Constellation integrated Dual-Frequency PPP (FCDF-PPP) solutions using observations at JFNG. The FCDF-PPP model developed by Cai et al. (2015) is adopted. It is clear that FCSF-PPP takes much longer than FCDF-PPP before its position solutions converge. If it is considered to have converged when the positioning errors reach 0·1 m and keep within 0·1 m, the position filter for FCSF-PPP needs 64·5, 73·5 and 85·0 minutes to converge in the east, north and up directions, respectively, while it needs only 21·5, 15·0 and 32·5 minutes for FCDF-PPP in the three directions. The RMS statistical values of position errors over the last 15 minutes are 0·3, 2·0 and 1·5 cm for FCSF-PPP and 0·3, 1·0 and 0·9 cm for FCDF-PPP in the three directions, respectively. It is indicated that FCSF-PPP still achieves a worse positioning accuracy than FCDF-PPP even after a long convergence time.

3.3. *Performance of FCSF-PPP in constrained visibility environments.* An accuracy improvement of only 1–2 mm was found after the integration with BeiDou and Galileo under an open sky, namely under the observing conditions with no signal blockage around

https://doi.org/10.1017/S0373463316000771 Published online by Cambridge University Press

the receiver, as shown in Figure 2. However, very often single-frequency PPP users are in environments with limited satellite visibility such as in urban canyons, mountainous areas and open-pit mines, etc. In order to investigate the performance of FCSF-PPP in these constrained visibility environments, the cut-off elevation angles are set from 20° to 50° in steps of 10° to simply simulate the real harsh environments. Figure 6 illustrates the positioning errors under different elevation mask angles using the dataset from JFNG. It is clearly seen that the vertical positioning errors increase rapidly with the increment of elevation mask angles whereas it is not the case for horizontal components. For the GPS-only case, the vertical accuracy starts to significantly degrade when the elevation mask angle increases to 20°. Similar situations are also found in the GPS/GLONASS case at a mask angle of 30°. By contrast, FCSF-PPP can still achieve better positioning performance at a mask angle of 40°. At a cut-off elevation angle of 50°, there are fairly large positioning errors in the vertical direction for all three processing cases, but FCSF-PPP still achieves the best positioning performance. The above phenomenon that the vertical accuracy decreases rapidly as the cut-off elevation angle increases may be explained by satellite sky distribution. The average Dilution of Precision (DOP) values in the horizontal and vertical components, namely HDOP and VDOP, are calculated. The average HDOP values for FCSF-PPP are 0·7, 0·9, 1·4 and 2·4 at cut-off angles from 20° to 50°, respectively, whereas the corresponding VDOP values are 1·4, 2·2, 4·6 and 8·9. The RMS statistics of positioning errors over the last 15 minutes as well as the average number of satellites under different elevation mask angles are given in Table 1. According to the statistical results, the three-dimensional (3D) accuracy improvement for the GPS/GLONASS case over the GPS-only case is 40%, 41%, 67% and 26%, and for the four-constellation case over the GPS/GLONASS case is 80%, 77%, 23% and 45% when the satellite elevation mask angle is set to 20°, 30°, 40° and 50°, respectively.

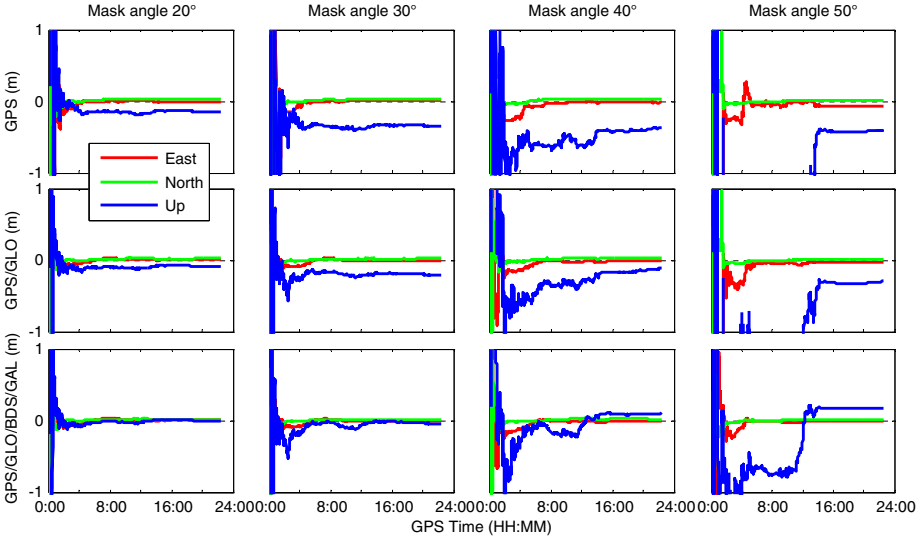

Figure 6. Single-frequency PPP positioning errors for three different constellation combinations under different elevation mask angles at JFNG on 7 April 2015.

https://doi.org/10.1017/S0373463316000771 Published online by Cambridge University Press

Table 1. RMS statistics of positioning errors and average number of satellites for three different constellation combinations under different elevation mask angles at JFNG on 7 April 2015.

		GPS	GPS/GLO	GPS/GLO/BDS/GAL
20°	East (cm)	0·4	0·3	0·3
	North (cm)	2·6	2·1	1·7
	Up (cm)	15·4	9·1	0·7
	Num. of Sats.	6·4	11·6	21·9
30°	East (cm)	0·5	0·3	0·2
	North (cm)	2·6	2·1	1·6
	Up (cm)	34·4	20·3	4·5
	Num. of Sats.	5·0	9·0	17·0
40°	East (cm)	2·0	1·1	0·7
	North (cm)	3·0	2·4	2·0
	Up (cm)	37·6	12·0	9·2
	Num. of Sats.	3·8	6·6	12·6
50°	East (cm)	6·8	3·5	1·8
	North (cm)	1·7	1·3	1·3
	Up (cm)	41·7	30·9	17·0
	Num. of Sats.	2·6	4·3	8·6

3.4. *Global FCSF-PPP accuracy assessment.* In order to assess the positioning accuracy of the FCSF-PPP in both static and kinematic modes, the FCSF-PPP solutions are compared with cases of GPS-only and GPS/GLONASS using datasets collected at 47 globally distributed four-system MGEX stations on seven consecutive days. Table 2 provides the statistical results of the static single-frequency PPP solutions for three different processing cases with different session lengths of 15 and 30 min, 1, 2, 4, 6 and 12 h. The RMS values are calculated from all static single-frequency PPP solutions over all the

Table 2. RMS values of static single-frequency PPP solutions for three different constellation combinations with different session lengths of 15 min, 30 min, 1 h, 2 h, 4 h, 6 h and 12 h.

		15 min	30 min	1 h	2 h	4 h	6 h	12 h
GPS (cm)	East	138·8	54·2	24·2	10·0	4·8	3·0	2·2
	North	83·2	33·1	18·4	7·1	2·8	2·1	1·7
	Up	223·6	73·6	30·1	11·2	7·3	5·1	3·1
	Horizontal	161·8	63·5	30·4	12·3	5·6	3·7	2·8
	3D	276·0	97·3	42·8	16·6	9·1	6·3	4·2
GPS/GLO (cm)	East	90·1	38·6	16·8	7·7	3·3	2·2	1·6
	North	59·9	19·2	10·2	4·6	2·1	1·6	1·3
	Up	144·2	49·7	20·6	9·5	6·1	3·8	2·3
	Horizontal	108·2	43·1	19·7	9·0	3·9	2·7	2·1
	3D	180·3	65·8	28·5	13·1	7·2	4·7	3·1
GPS/GLO/BDS/GAL (cm)	East	83·3	24·9	13·5	5·7	3·0	1·6	1·2
	North	53·6	17·6	9·6	3·7	1·8	1·2	1·0
	Up	118·6	41·5	16·1	7·2	4·6	2·7	1·6
	Horizontal	99·1	30·5	16·6	6·8	3·5	2·0	1·6
	3D	154·5	51·5	23·1	9·9	5·7	3·3	2·2

https://doi.org/10.1017/S0373463316000771 Published online by Cambridge University Press

selected stations and days. It can be seen that the positioning accuracy is continuously improved along with the increase of observational length. With the same session length, the four-constellation integrated case achieves the highest positioning accuracy, and the GPS/GLONASS case follows. Usually, the positioning accuracy in the north coordinate component is the best, while the vertical component is the most inaccurate component. The GPS-only single-frequency PPP requires more than two hours to achieve a positioning accuracy better than 10 cm for all three coordinate components. As to the other two cases, an accuracy better than 10 cm for all three components is available within two hours. In addition, the FCSF-PPP can also achieve a 3D positioning accuracy better than 10 cm within two hours. After undergoing a long convergence time of 12 hours, the 3D positioning accuracy for GPS-only, GPS/GLONASS and four-constellation cases is 4·2, 3·1 and 2·2 cm, respectively. The correlation between coefficient matrices of adjacent epochs is very high. Therefore, the repeat observation in a short period of time will do little to help the convergence of parameters or the improvement of accuracy because of the small changes in satellite sky distribution. In contrast, a long observation time of up to 12 hours can be very helpful, which benefits from the availability of numerous measurements and the strong satellite geometry. For comparison, the RMS values are also calculated from all static FCDF-PPP solutions. The 3D positioning accuracy for four-constellation integrated dual-frequency case with seven different session lengths is 37·7, 15·6, 6·5, 3·9, 2·3, 1·6 and 0·7 cm, respectively.

For the purpose of evaluating the positioning accuracy of kinematic FCSF-PPP solutions, the station coordinates are estimated epoch-by-epoch without imposing any constraints between the epochs. Figure 7 depicts the distribution of kinematic positioning errors, number of satellites and PDOP for GPS-only, GPS/GLONASS and four-constellation processing cases. All data are processed in kinematic mode, and each error value in Figure 7 refers to the positioning error at an epoch. As the position solutions in

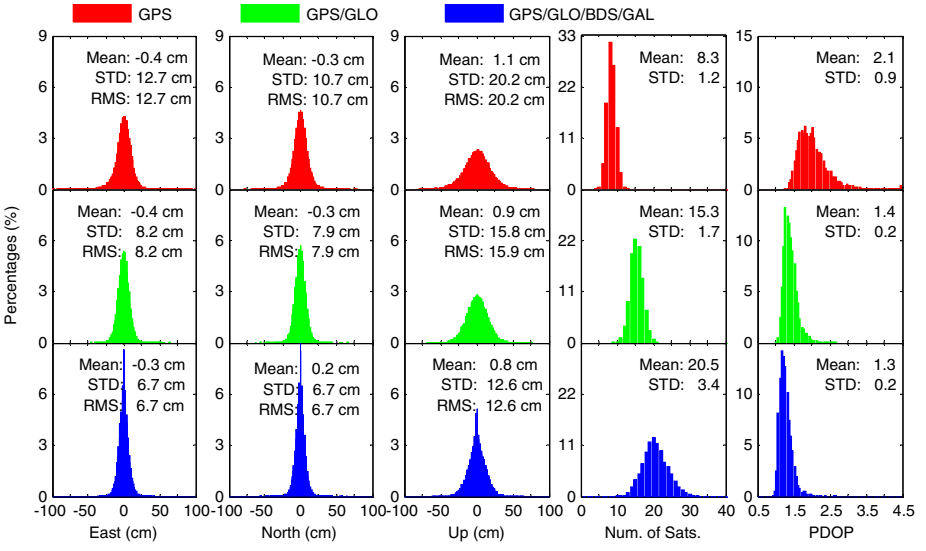

Figure 7. Distribution of epoch-wise kinematic positioning errors, number of satellites and PDOP for three different constellation combinations.

https://doi.org/10.1017/S0373463316000771 Published online by Cambridge University Press

the first two hours are still in the converging stage, they are not used for the kinematic accuracy statistics. It is clearly seen that the positioning errors in all three directions are approximately normally distributed. The four-constellation case accounts for the largest percent of smaller errors, and the GPS/GLONASS case follows. The statistical results in terms of mean values, Standard Deviation (STD) values and RMS values are also given in Figure 7. According to the RMS values, the improvement of the GPS/GLONASS case on the positioning accuracy is 35%, 26% and 21% over the GPS-only case in the east, north and up directions, respectively. Furthermore, the accuracy improvement of FCSF-PPP over GPS/GLONASS single-frequency PPP is 18%, 15% and 21% in the three directions, respectively. The kinematic positioning accuracy for the FCSF-PPP is 6·7, 6·7 and 12·6 cm in the three directions, respectively. The average number of satellites and PDOP values for the above three processing cases are 8·3, 15·3 and 20·5, and 2·1, 1·4 and 1·3, respectively.

The positioning errors of single-frequency PPP in kinematic mode are larger than those in static mode. For the purpose of the convergence analysis, the precision threshold is set to 0·5 m for the east and north directions and 1 m for the up direction, respectively. The average convergence time for all single-day kinematic solutions of single-frequency PPP is presented in Table 3. The improvement of the FCSF-PPP on the convergence time is 41%, 37% and 55% over the GPS-only case and 13%, 11% and 23% over the GPS/GLONASS case in the east, north and up directions, respectively.

Since the current BeiDou system is in the stage of regional deployment, the BeiDou satellites are still not globally evenly distributed. In addition, only a few Galileo satellites are available under the current Galileo constellation, leading to the quite different visibility of Galileo satellites in the global scale. In order to truly evaluate the contributions of BeiDou and Galileo systems, Figure 8 shows the 3D accuracy improvement against the PDOP improvement after adding BeiDou and Galileo observations to the GPS/GLONASS single-frequency PPP processing in kinematic mode. Only the results at a certain epoch that includes at least two BeiDou satellites or two Galileo satellites are involved in the statistics. The RMS statistics of 3D positioning errors and average PDOP values over all the available epochs at each selected station on each selected day are calculated respectively, and thus there is a total of 329 blue points in Figure 8. The red line shown in Figure 8 is the linear fitting of the blue points, which reveals a trend that the 3D accuracy improvement rates increase as the PDOP improvement rates increase. This demonstrates that the improvement of positioning accuracy is dependent on the improvement of satellite sky distribution.

3.5. *Kinematic results and analysis.* The kinematic accuracy evaluation shown in the previous section is implemented by processing the static measurements with the strategies adopted in kinematic mode. In order to assess the FCSF-PPP performance in the real kinematic mode, a kinematic experiment was conducted within the new campus of the Central South University in Changsha, China, on 16 August 2014. The experiment started at the local time 18:00 (GPS time 10:00) and lasted for two hours. The experiment time was

Table 3. Convergence time for single-frequency PPP kinematic solutions (min).

	East	North	Up
GPS	53·2	30·8	87·3
GPS/GLO	36·2	21·8	50·6
GPS/GLO/BDS/GAL	31·5	19·5	39·2

https://doi.org/10.1017/S0373463316000771 Published online by Cambridge University Press

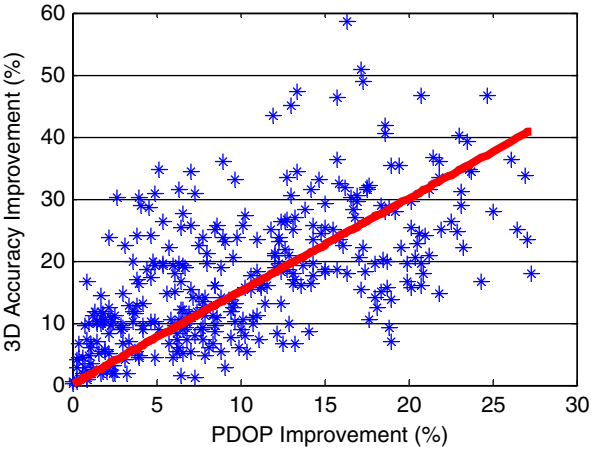

Figure 8. Dependence of 3D accuracy improvement on the PDOP improvement after adding BeiDou and Galileo observations to the GPS/GLONASS single-frequency PPP processing in kinematic mode.

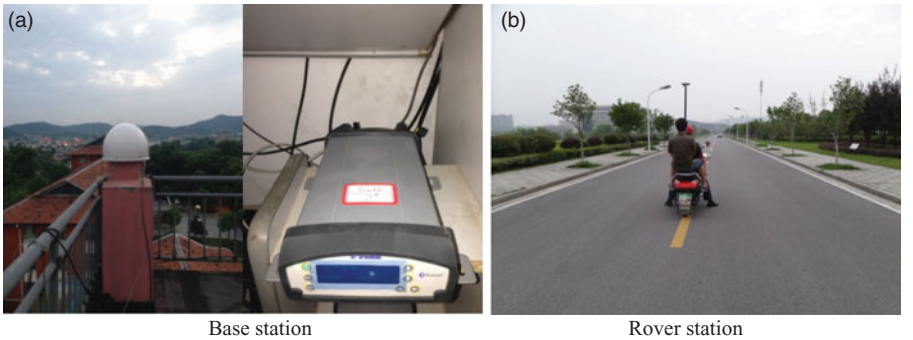

Base station Rover station

Figure 9. Field observation equipment and environment for FCSF-PPP kinematic experiment on 16 August 2014.

planned in advance so that all three operational Galileo IOV satellites at that time could be tracked in the experimental area. Figure 9 shows the field observation equipment and environment for both base and rover stations. At the rover station, a "Trimble NetR9" GNSS receiver with a "Trimble Zephyr Model 2" geodetic antenna was carried by an electric bicycle to collect kinematic data from four constellations. The moving vehicle was driven at a speed of around 10 km/h. At the base station, the same type of receiver with a "TRM55971.00" antenna and a radome was set up on the roof of the Mining Building of the Central South University to help determine the reference coordinates of the rover station at cm level accuracy using a double-difference Real-Time Kinematic (RTK) approach. The distance between the base and rover stations was less than 2·5 km. The kinematic data was collected at a sampling interval of 1 s. The satellite elevation mask angle was set to 10°.

Figure 10 shows the kinematic positioning errors of GPS-only, GPS/GLONASS and four-constellation single-frequency PPP solutions with respect to the reference coordinate

https://doi.org/10.1017/S0373463316000771 Published online by Cambridge University Press

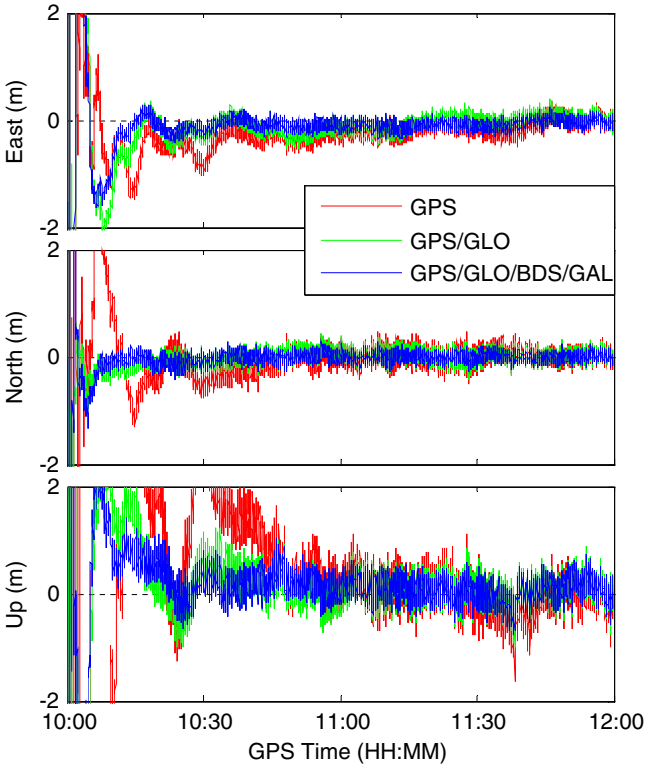

Figure 10. Single-frequency PPP kinematic positioning errors for three different constellation combinations in the kinematic experiment.

values in the east, north and up directions. Figure 11 presents the corresponding number of satellites and PDOP. The average number of satellites and PDOP values for the above three processing cases are 8·4, 14·2 and 24·2, and 1·9, 1·4 and 1·2, respectively. It is obvious that the positioning errors are significantly reduced for the GPS/GLONASS case over the GPS-only case, especially in the vertical direction. The positioning accuracy is further improved after a further integration with BeiDou and Galileo. The RMS statistical values are computed using the positioning errors in the last one hour in which the position solutions in all three directions have reached stable values. GPS-only single-frequency PPP has the worst positioning accuracy with RMSs of 18·6, 13·7 and 33·2 cm in the east, north and up directions, respectively. With the combination of GPS and GLONASS, the positioning accuracy is improved by 30%, 20% and 28% over the GPS-only case to 13·0, 10·9 and 23·9 cm in the three directions, respectively. The FCSF-PPP improves the positioning accuracy by 11%, 28% and 13% over the GPS/GLONASS single-frequency PPP to 11·6, 7·8 and 20·9 cm in the three directions, respectively. When using dual-frequency observations, the four-constellation case can achieve an accuracy of 4·0, 2·1 and 9·6 cm in the three directions, respectively. Compared with the results shown in Figure 7, it is indicated that the positioning accuracy in the real kinematic mode is worse than that in the simulated kinematic mode.

https://doi.org/10.1017/S0373463316000771 Published online by Cambridge University Press

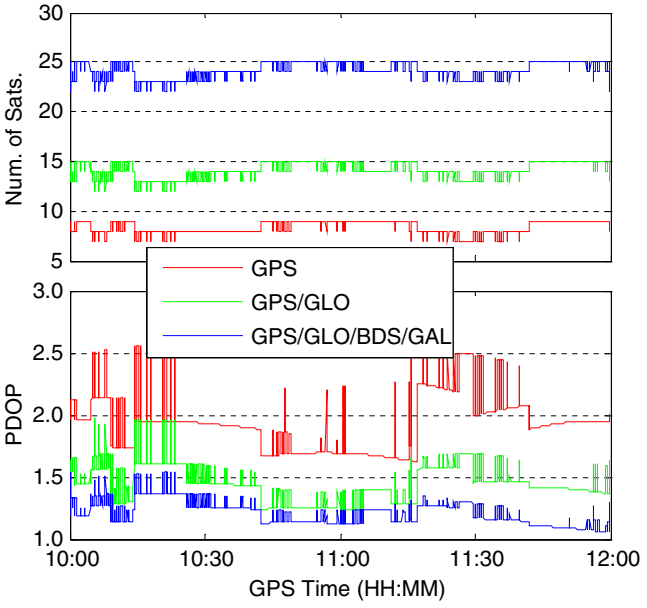

Figure 11. Number of satellites and PDOP for three different constellation combinations in the kinematic experiment.

4. CONCLUSIONS. For most positioning and navigation applications, single-frequency GNSS receivers are widely used due to the low costs. Therefore the high-precision single-frequency PPP technique has attracted great interest in the GNSS community. Multi-constellation integration has the potential to significantly improve the positioning accuracy and reduce the convergence time due to the increased number of visible satellites and the improved satellite sky distribution. Since BeiDou and Galileo have already begun to transmit signals for position determination, the four-constellation integrated single-frequency PPP has become feasible. In this study, a FCSF-PPP model based on the GRAPHIC ionosphere-free combination to remove the ionospheric effect is presented to simultaneously process the pseudorange and carrier phase observations on a single frequency from GPS, GLONASS, BeiDou and Galileo. Datasets from 47 globally distributed four-system MGEX stations on seven consecutive days as well as a kinematic experimental dataset are employed to fully assess the performance of FCSF-PPP. The performance of FCSF-PPP is compared to GPS-only and combined GPS/GLONASS single-frequency PPP.

Using the MGEX datasets, the statistical results indicate that the 3D positioning accuracy for the FCSF-PPP is 154·5, 51·5, 23·1, 9·9, 5·7, 3·3 and 2·2 cm with different session lengths of 15 and 30 min, 1, 2, 4, 6 and 12 h in the static mode, respectively. In the kinematic mode, the FCSF-PPP can achieve an accuracy of 6·7, 6·7 and 12·6 cm in the east, north and up directions, respectively. In addition, the positioning performance of the four-constellation case is better than that of the GPS-only and GPS/GLONASS cases. Both the BeiDou and Galileo constellations will be fully deployed in the next few years, and thus greater benefits from the four-constellation integration can be expected. It is noted that the presented results are obtained using multi-frequency geodetic-type receivers rather

https://doi.org/10.1017/S0373463316000771 Published online by Cambridge University Press

than single-frequency navigation-type receivers. If the latter ones are used, the positioning accuracy could degrade due to the relatively poorer data quality. Nevertheless, the exhibited results are a good indication of the FCSF-PPP performance under the current GNSS constellations.

Considering that an accuracy better than 2 cm after an observation time of 12 hours in static mode and 13 cm in kinematic mode can be achieved in all three coordinate components, FCSF-PPP has large implications for development of low-cost and high-precision applications, such as precision agriculture, vegetation boundaries, hydrography and navigation applications in the automotive markets. Future work includes tests of Real-Time Kinematic PPP (PPP-RTK) ambiguity resolution for a truly single-frequency low-cost receiver with the use of precise corrections comprising satellite clocks, satellite phase biases and ionospheric delays from a regional Continuously Operating Reference Station (CORS) network.

ACKNOWLEDGMENTS

The contribution of data from IGS and GFZ is appreciated. This study was supported by National Natural Science Foundation of China (Grant No. 41474025).

REFERENCES

Boehm, J., Niell, A., Tregoning, P. and Schuh, H. (2006). Global Mapping Function (GMF): a new empirical mapping function based on numerical weather model data. *Geophysical Research Letters*, **33**, L07304, DOI: 10.1029/2005GL025546.

Cai, C., Gao, Y., Pan, L. and Zhu, J. (2015). Precise point positioning with quad-constellations: GPS, BeiDou, GLONASS and Galileo. *Advances in Space Research*, **56**(1), 133–143, DOI: 10.1016/j.asr.2015.04.001.

Cai, C., Liu, Z. and Luo, X. (2013). Single-frequency ionosphere-free precise point positioning using combined GPS and GLONASS observations. *Journal of Navigation*, **66**(3), 417–434, DOI: 10.1017/S0373463313000039.

Davis, J.L., Herring, T.A., Shapiro, I.I., Rogers, A.E.E. and Elgered, G. (1985). Geodesy by radio interferometry: effects of atmospheric modeling errors on estimates of baseline length. *Radio Science*, **20**(6), 1593–1607, DOI: 10.1029/RS020i006p01593.

Gerdan, G.P. (1995). A comparison of four methods of weighting double difference pseudorange measurements. *The Australian Surveyor*, **40**(4), 60–66, DOI: 10.1080/00050334.1995.10558564.

Ghoddousi-Fard, R. and Dare, P. (2006). Online GPS processing services: an initial study. *GPS Solutions*, **10**(1), 12–20, DOI: 10.1007/s10291-005-0147-5.

Guo, F., Zhang, X. and Wang, J. (2015). Timing group delay and differential code bias corrections for BeiDou positioning. *Journal of Geodesy*, **89**(5), 427–445, DOI: 10.1007/s00190-015-0788-2.

Héroux, P. and Kouba, J. (1995). GPS precise point positioning with a difference. In: *Geomatics '95*, Ottawa, Ontario, Canada, June 13–15, 1995.

Hauschild, A., Montenbruck, O., Sleewaegen, J.M., Huisman, L. and Teunissen, P.J.G. (2012). Characterization of Compass M-1 signals. *GPS Solutions*, **16**(1), 117–126, DOI: 10.1007/s10291-011-0210-3.

Kouba, J. and Héroux, P. (2001). Precise point positioning using IGS orbit and clock products. *GPS Solutions*, **5**(2), 12 –28, DOI: 10.1007/PL00012883.

Le, A.Q. and Tiberius, C. (2007). Single-frequency precise point positioning with optimal filtering. *GPS Solutions*, **11**(1), 61–69, DOI: 10.1007/s10291-006-0033-9.

Li, X., Zhang, X. and Ge, M. (2011). Regional reference network augmented precise point positioning for instantaneous ambiguity resolution. *Journal of Geodesy*, **85**(3), 151–158, DOI: 10.1007/s00190-010-0424-0.

Li, X., Ge, M., Zhang, H. and Wickert, J. (2013a). A method for improving uncalibrated phase delay estimation and ambiguity-?xing in real-time precise point positioning. *Journal of Geodesy*, **87**(5), 405–416, DOI: 10.1007/s00190-013-0611-x.

Li, X., Ge, M., Zhang, H., Nischan, T. and Wickert, J. (2013b). The GFZ real-time GNSS precise positioning service system and its adaption for COMPASS. *Advances in Space Research*, **51**(6), 1008–1018, DOI: 10.1016/j.asr.2012.06.025.

Li, X., Zhang, X., Ren, X., Fritsche, M., Wickert, J. and Schuh, H. (2015a). Precise positioning with current multi-constellation global navigation satellite systems: GPS, GLONASS, Galileo and BeiDou. *Scientific Reports*, **5**, 8328, DOI: 10.1038/srep08328.

Li, X., Ge, M., Dai, X., Ren, X., Fritsche, M., Wickert, J. and Schuh, H. (2015b). Accuracy and reliability of multi-GNSS real-time precise positioning: GPS, GLONASS, BeiDou, and Galileo. *Journal of Geodesy*, **89**(6), 607–635, DOI: 10.1007/s00190-015-0802-8.

Montenbruck, O. (2003). Kinematic GPS positioning of LEO satellites using ionosphere-free single frequency measurements. *Aerospace Science and Technology*, **7**(5), 396–405, DOI: 10.1016/S1270-9638(03)00034-8.

Montenbruck, O., Hauschild, A., Steigenberger, P., Hugentobler, U., Teunissen, P. and Nakamura, S. (2013). Initial assessment of the COMPASS/BeiDou-2 regional navigation satellite system. *GPS Solutions*, **17**(2), 211–222, DOI: 10.1007/s10291-012-0272-x.

Øvstedal, O. (2002). Absolute positioning with single-frequency GPS receivers. *GPS Solutions*, **5**(4), 33–44, DOI: 10.1007/PL00012910.

Pan, L., Cai, C., Santerre, R. and Zhu, J. (2014). Combined GPS/GLONASS precise point positioning with fixed GPS ambiguities. *Sensors*, **14**(9), 17530–17547, DOI: 10.3390/s140917530.

Rizos, C., Montenbruck, O., Weber, R., Weber, G., Neilan, R. and Hugentobler, U. (2013). The IGS MGEX experiment as a milestone for a comprehensive multi-GNSS service. *Proceedings of the ION 2013 Pacific PNT Meeting (ION-PNT-2013)*, April 23–25, 2013, Honolulu, Hawaii, USA, 289–295.

Saastamoinen, J. (1972). Atmospheric correction for the troposphere and stratosphere in radio ranging of satellites. *The Use of Artificial Satellites for Geodesy*, American Geophysics Union, Geophys. Monogr. Ser., **15**, 247–251.

Steigenberger, P., Hugentobler, U., Loyer, S., Perosanz, F., Prange, L., Dach, R., Uhlemann, M., Gendt, G. and Montenbruck, O. (2015). Galileo orbit and clock quality of the IGS multi-GNSS experiment. *Advances in Space Research*, **55**(1), 269–281, DOI: 10.1016/j.asr.2014.06.030.

Sterle, O., Stopar, B. and Prešeren, P.P. (2015). Single-frequency precise point positioning: an analytical approach. *Journal of Geodesy*, **89**(8), 793–810, DOI: 10.1007/s00190-015-0816-2.

Wanninger, L. and Beer, S. (2015). BeiDou satellite-induced code pseudorange variations: diagnosis and therapy. *GPS Solutions*, **19**(4), 639–648, DOI: 10.1007/s10291-014-0423-3.

Yunck, T.P. (1996). Orbit determination. In: Parkinson, B.W., Spilker, J.J. (eds). *Global positioning system – theory and applications*. AIAA, Washington D.C., USA.

Zhao, Q., Guo, J., Li, M., Qu, L., Hu, Z., Shi, C. and Liu, J. (2013). Initial results of precise orbit and clock determination for COMPASS navigation satellite system. *Journal of Geodesy*, **87**(5), 475–486, DOI: 10.1007/s00190-013-0622-7.

Zumberge, J.F., Heflin, M.B., Jefferson, D.C., Watkins, M.M. and Webb, F.H. (1997). Precise point positioning for the efficient and robust analysis of GPS data from large networks. *Journal of Geophysical Research*, **102**(B3), 5005–5017, DOI: 10.1029/96JB03860.